Supporting Information

Covalent Organic Framework as a Nanocarrier for Synergistic Phototherapy and Immunotherapy

Ying Zhou,[ab] *Sainan Liu,*[ac] *Chunling Hu,*[ac] *Lihan Cai*[ac] *and Maolin Pang**[ac]

[a] *State Key Laboratory of Rare Earth Resource Utilization, Changchun Institute of Applied Chemistry, Chinese Academy of Sciences, Changchun 130022, P. R. China*
[b] *School of Chemistry & Environmental Engineering, Changchun University of Science and Technology, Changchun, 130022, P. R. China*
[c] *University of Science and Technology of China, Hefei, Anhui 230026, P. R. China*

*Corresponding author
E-mail: mlpang@ciac.ac.cn

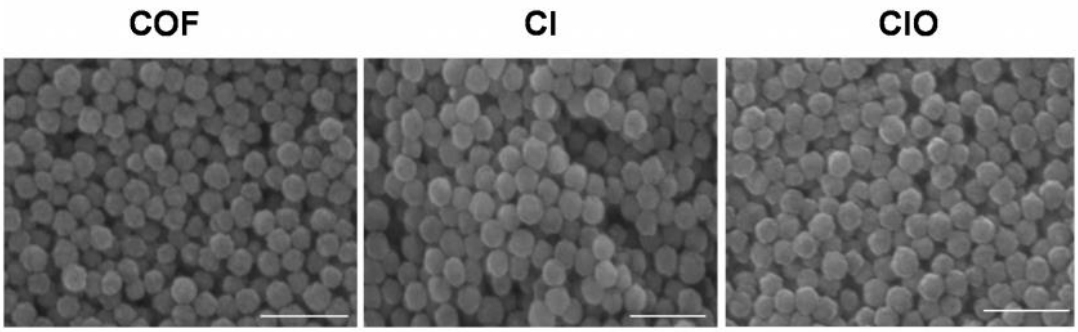

Fig. S1 SEM image (Scale bar = 500 nm) of COF, CI and CIO nanoparticles.

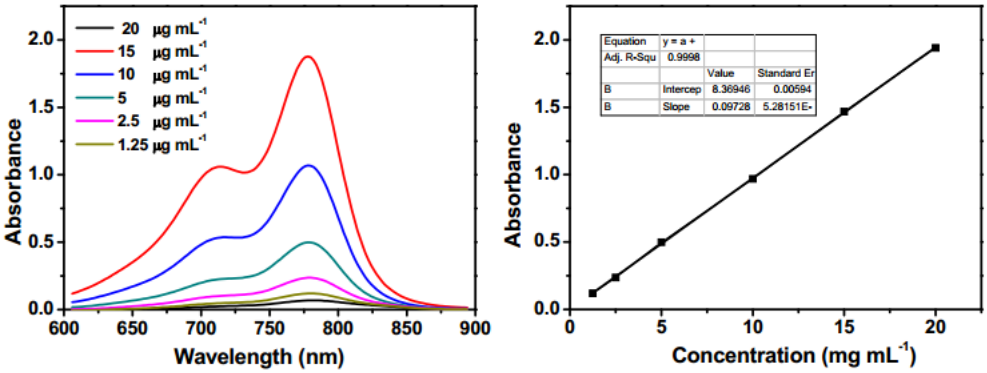

Fig. S2 Quantitative measurement of ICG loading efficiency based on the UV-Vis spectra. The absorbance intensity at 780 nm was correlated with the ICG in concentration. The obtained standard curve is y = 0.09728x + 0.00083946, R^2= 0.99985 (y: absorbance value at 780 nm; x: concentration of ICG)

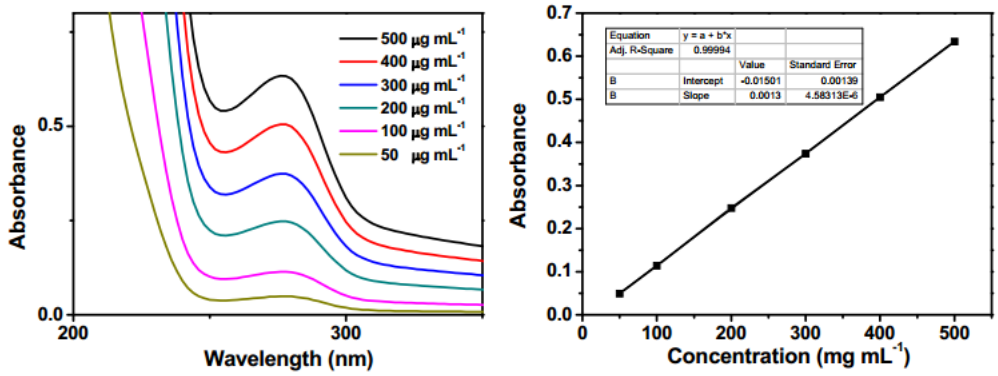

Fig. S3 Quantitative measurement of OVA loading efficiency based on the UV-Vis spectra. The absorbance intensity at 280 nm was correlated with the OVA in concentration. The obtained standard curve is y = 0.0031x - 0.01501, R^2= 0.99994 (y: absorbance value at 280 nm; x: concentration of OVA)

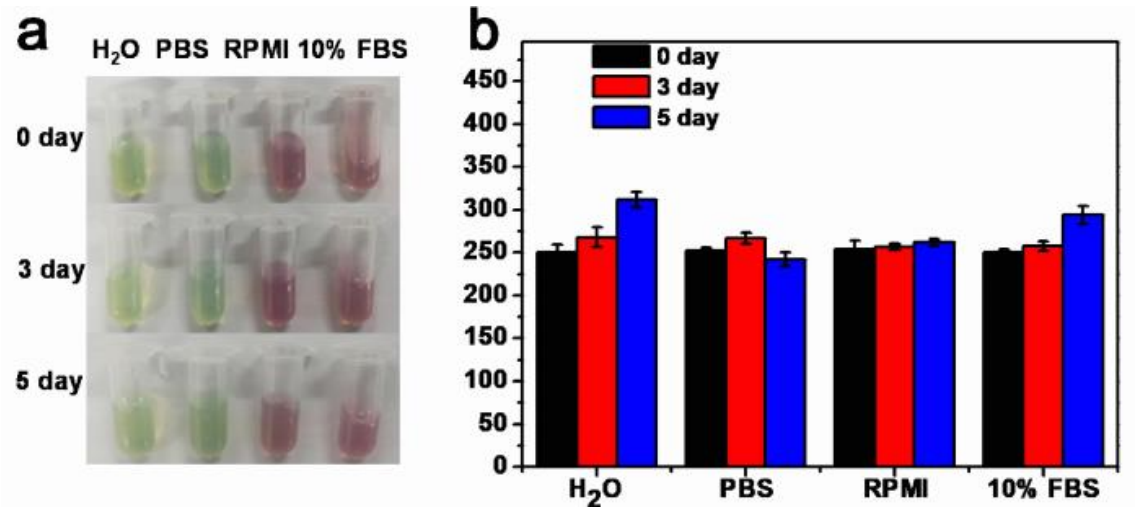

Fig. S4 (a) Images of the CIO nanoparticles dispersed in various solutions for 0-5 days. (b) DLS measurements of CIO nanoparticles incubated with pure H_2O, PBS, RPMI-1640 and 10% FBS at 37 ^{o}C for 0, 3, 5 days, respectively. The data represents mean ± SD (n = 3).

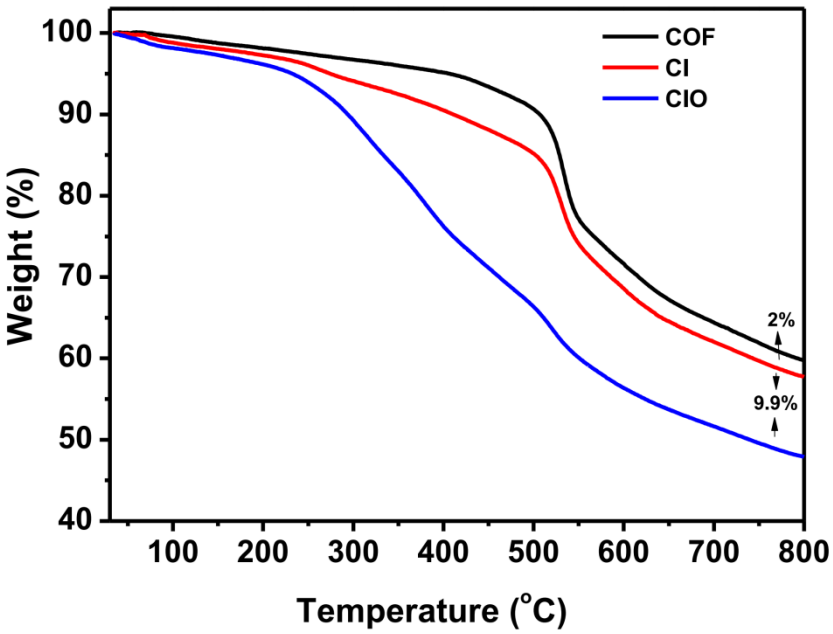

Fig. S5 Thermogravimetric analysis (TGA) curves for COF, CI and CIO.

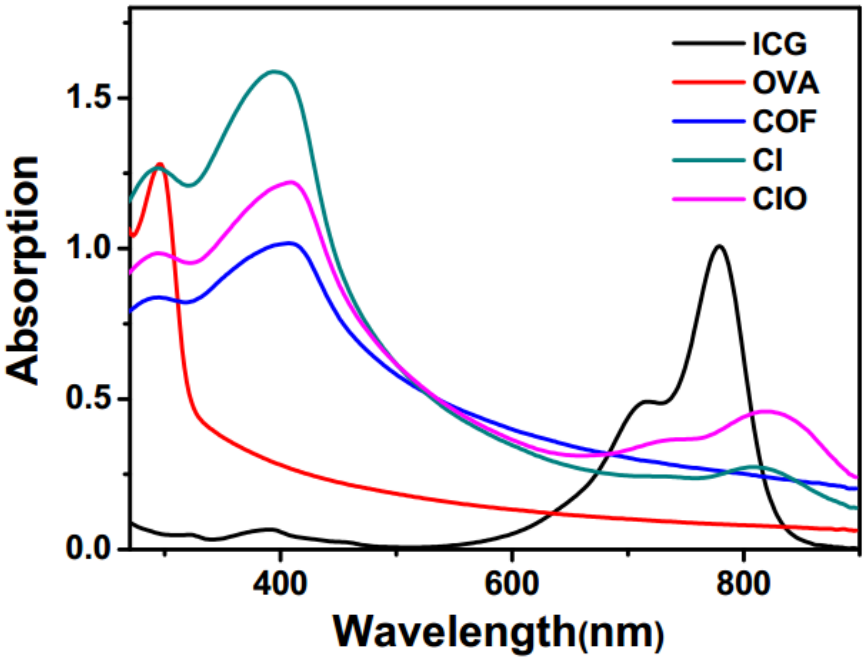

Fig. S6 UV-vis spectra of ICG, OVA, COF, CI and CIO, respectively.

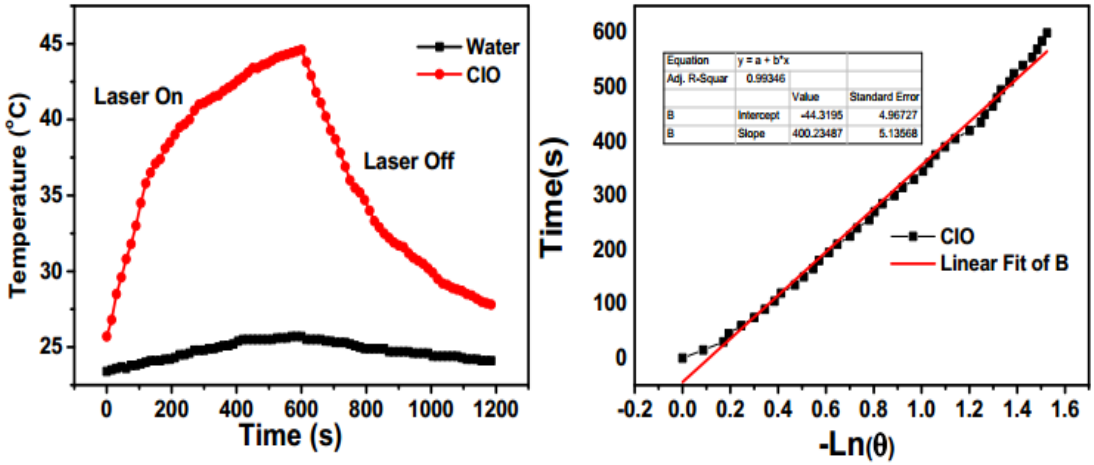

Fig. S7 Photothermal effect of CIO aqueous solution (100 μg mL^{-1}) irradiated with an 808 nm CW laser (1.09 W cm^{-2}). Linear fit of time/-ln(θ) obtained during the cooling process.

Table S1 Photothermal conversion efficiency for CIO. Absorbance at irradiation wavelength (A_{808} nm), mass of solution (m sol), increasing temperature after CW laser irradiation (ΔT), time system constant (τs), thermal conductance (hS) and photothermal conversion efficiency (Efficiency).

Abs 808 nm	m sol (g)	ΔT (K)	T_s (s)	hS (WK^{-1})	Efficiency(%)
0.684	1	18.9	400.2348	0.0105	35.76%

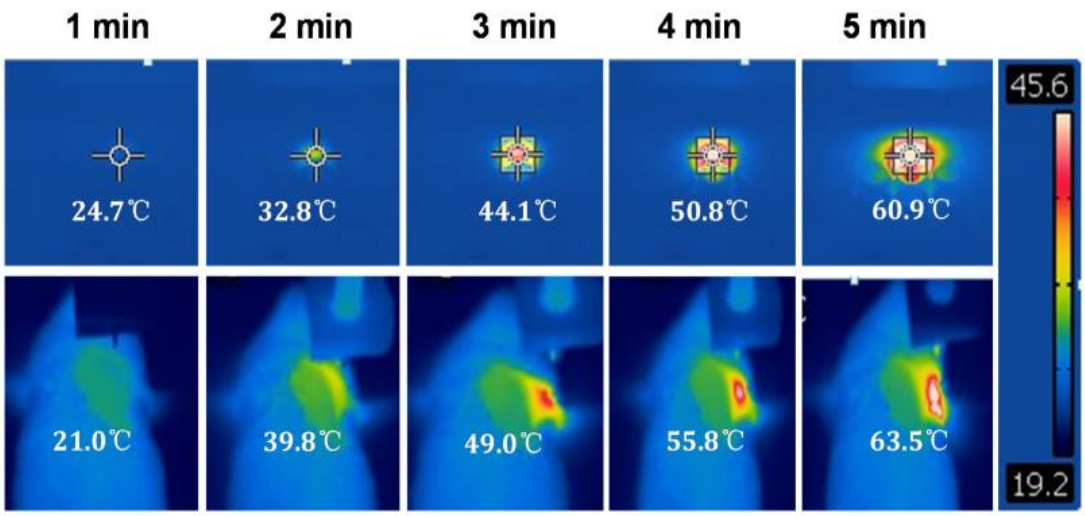

Fig. S8 Photographs of CIO (200 μg mL^{-1}, in water) upon laser irradiation for different times. The whole body photothermal images of mice after intratumoral injection of CIO (0.1 mL, 200 μg mL^{-1}). Laser irradiation conditions: 808 nm and 1.09 W cm^{-2}.

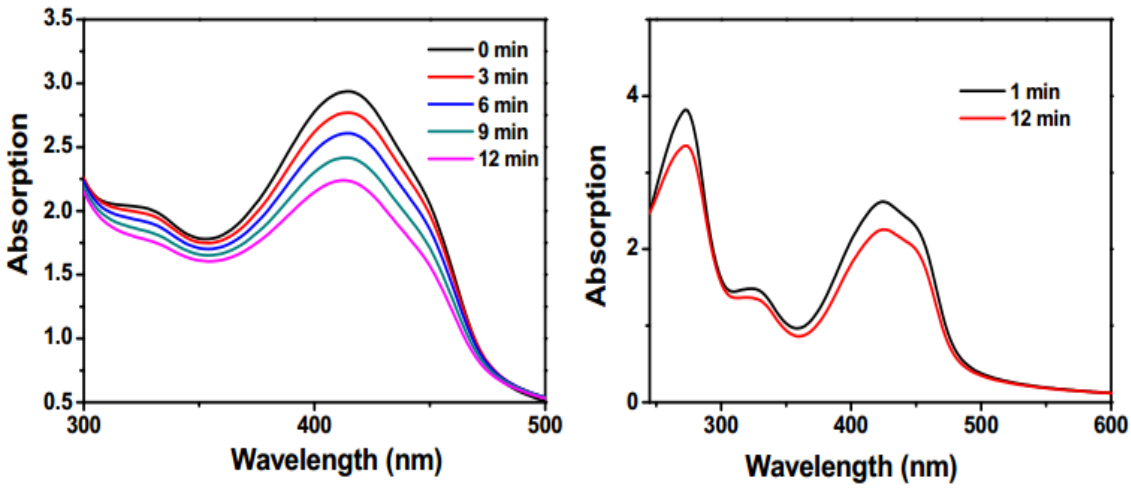

Fig. S9 UV spectra of DPBF solution in the presence of CIO nanoparticles and absence under laser irradiation (650 nm, 0.72 W cm^{-2}, 12 min).

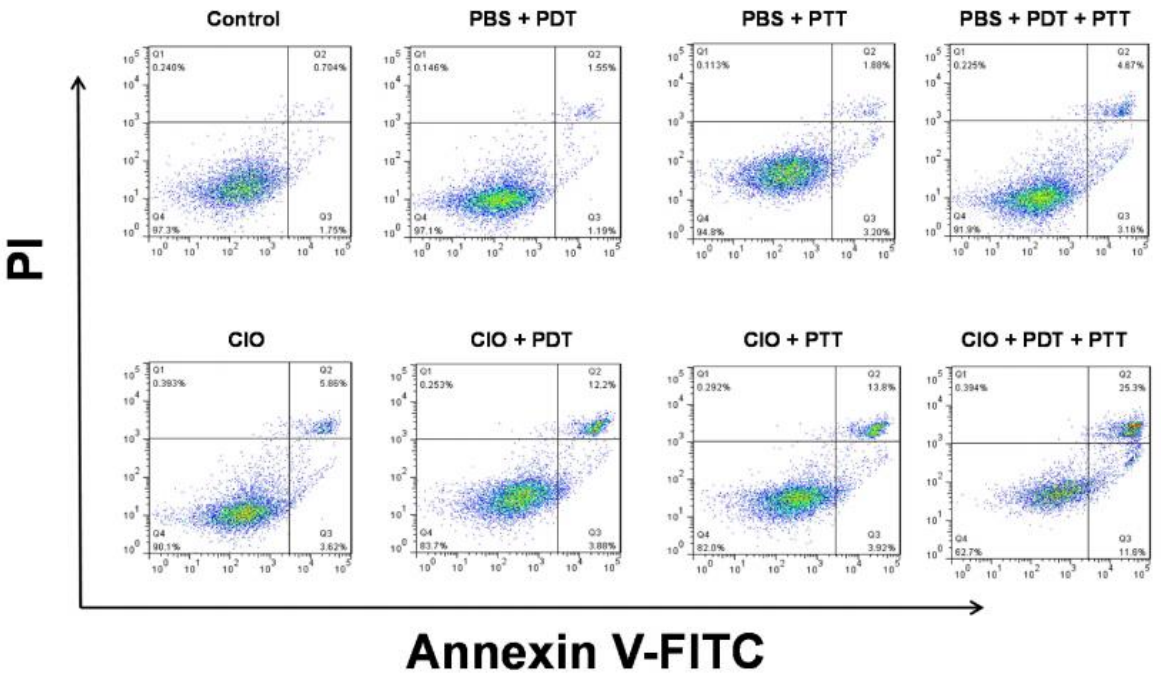

Fig. S10 Flow cytometry assays of CT26 cells treated with different methods.

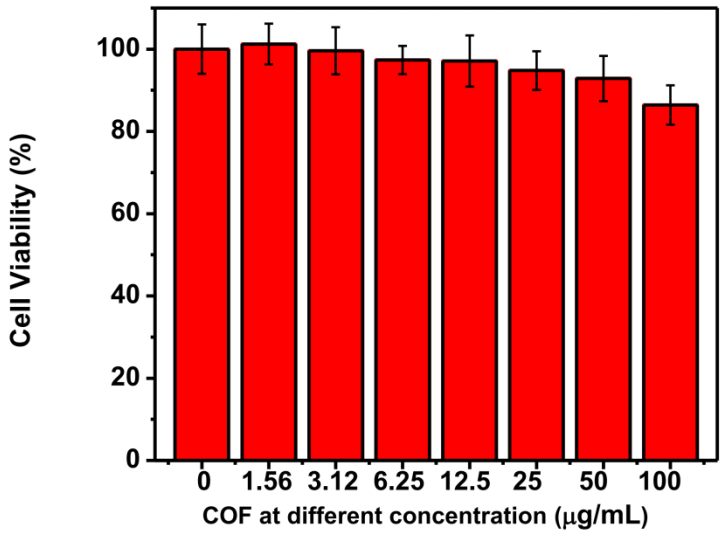

Fig. S11 Cytotoxicity assay of L929 cells incubated with COF at different concentrations (0, 1.56, 3.12,6.25,12.5, 25, 50, and 100 μg mL^{-1}) for 24 h.

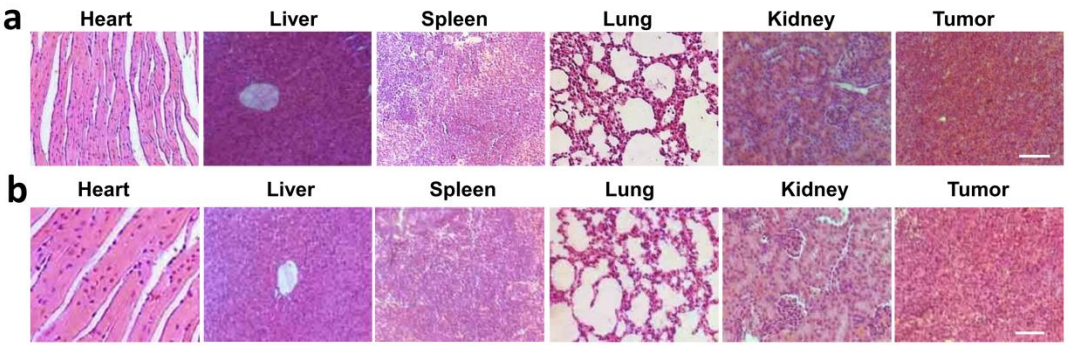

Fig.S12 H&E stained images of heart, liver, spleen, lung, kidney and tumor from the tumor-bearing mice treated with (a) COF and (b) CIO, the scale bar is 50 μm.

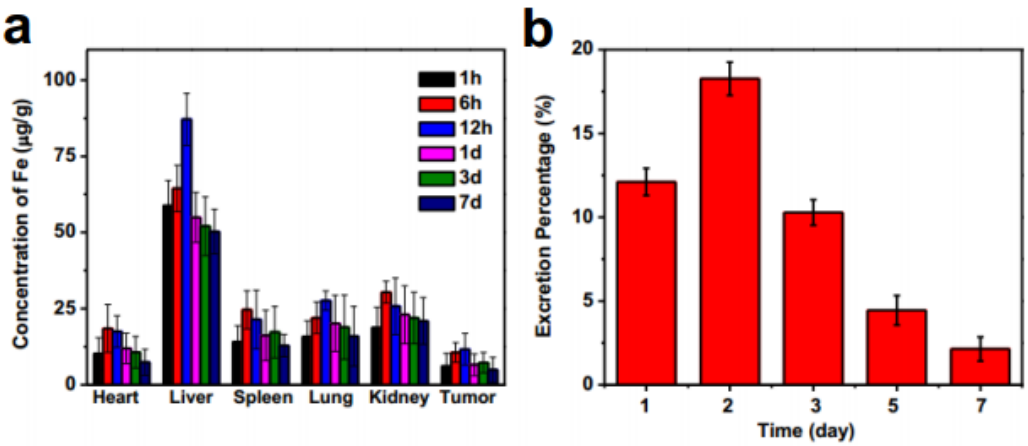

Fig. S13 (a) The in vivo biodistribution and (b) the contents of Fe in feces after injection with CIO nanoparticles intravenously for different times.

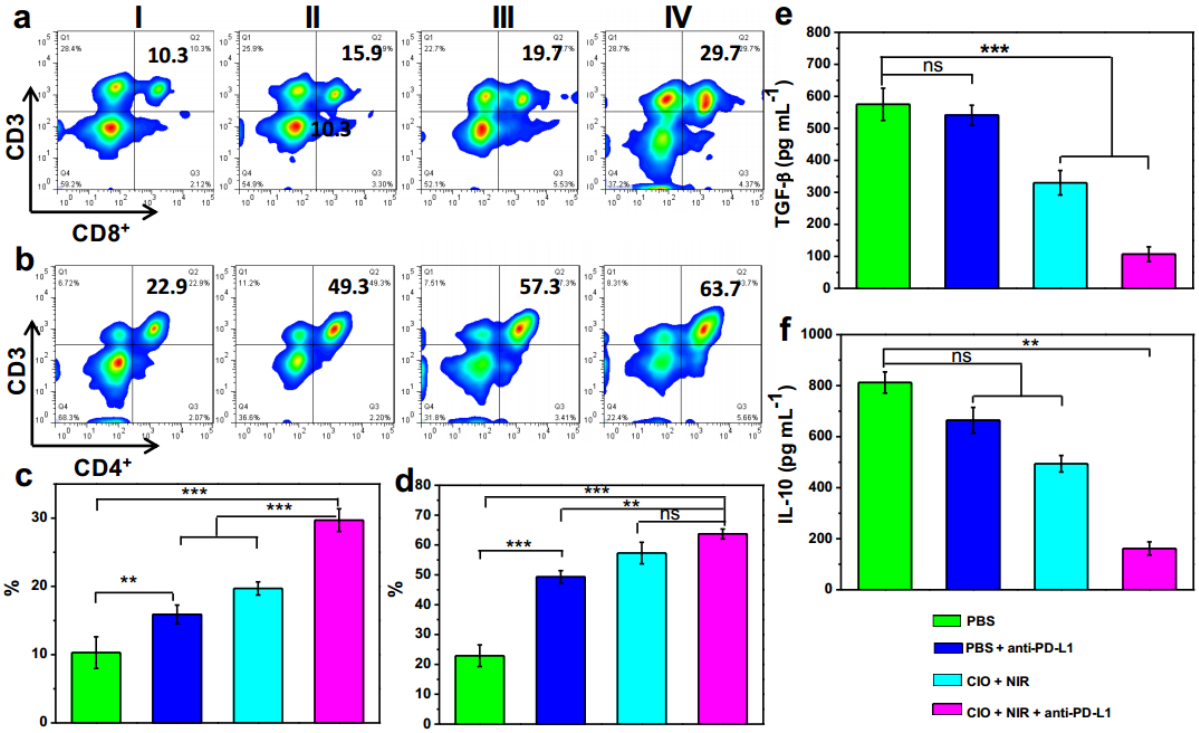

Fig. S14 (a) The flow cytometric analyses of the populations of CD8+ (CD3+CD8+ as the marker) T cells in lymph node of mice. I, PBS; II, PBS + anti-PD-L1; III, CIO + PDT + PTT; IV, CIO + PDT + PTT + anti-PD-L1. (b) The flow cytometric analyses of the populations of CD4+ (CD3+CD4+ as the marker) T cells in lymph node of mice after various treatments. (c) Data of CD3+CD4+ and (d) CD3+CD8+ were expressed as mean ± SD (n= 3) (*p < 0.05; **p < 0.01; ***p < 0.001). (e) The secretion level of IL-10 and (f) TGF-β1tumors obtained from immunized mice. ANOVA was used to assess statistical significance: *p < 0.5, **p < 0.01, ***p < 0.001.

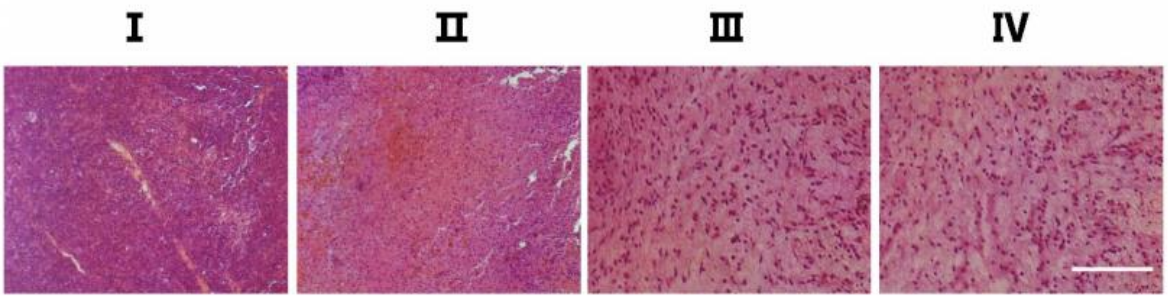

Fig. S15 H&E stained images of tumor with PBS, PBS + anti-PD-L1, CIO + PDT + PTT and CIO + PDT + PTT + anti-PD-L1 treatments (scale bar is 200 μm).

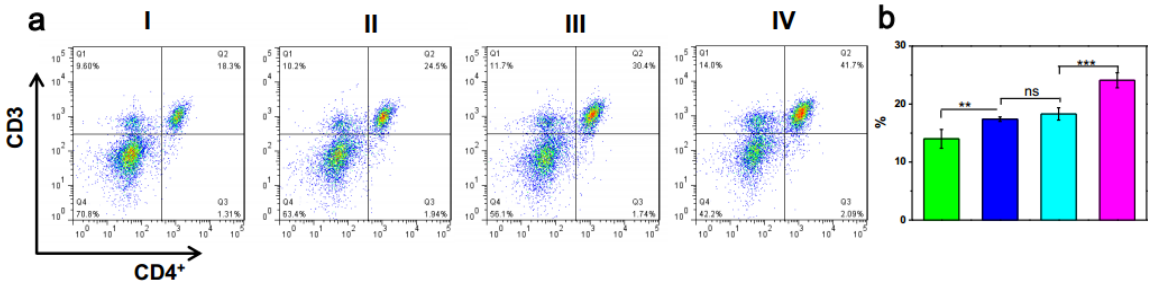

Fig. S16 (a) The flow cytometric analyses of the populations of CD4+ (CD3+CD4+ as the marker) T cells in spleens of mice after various treatments. I, PBS; II, PBS + anti-PD-L1; III, CIO + PDT + PTT; IV, CIO + PDT + PTT + anti-PD-L1. (b) Data of CD3+CD4+ was expressed as mean ± SD (n= 3) (*p < 0.05; **p < 0.01; ***p < 0.001). (Green is PBS group; Mazarine blue is PBS + anti-PD-L1; Blue is CIO + PDT + PTT; Pink is CIO + PDT + PTT + anti-PD-L1)

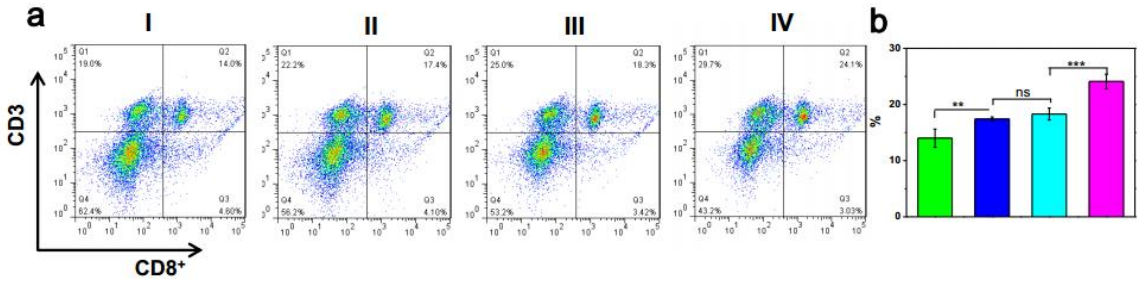

Fig. S17 (a) The flow cytometric analyses of the populations of CD8+ (CD3+CD8+ as the marker) T cells in spleens of mice after various treatments. I, PBS; II, PBS + anti-PD-L1; III, CIO + PDT + PTT; IV, CIO + PDT + PTT + anti-PD-L1. (b) Data of CD3+CD8+ was expressed as mean ± SD (n= 3) (*p < 0.05; **p < 0.01; ***p < 0.001). (Green is PBS group; Mazarine blue is PBS + anti-PD-L1; Blue is CIO + PDT + PTT; Pink is CIO + PDT + PTT + anti-PD-L1)